Inorganic Chemistry

Forum Article

pubs.acs.org/IC

C−H Bond Cleavage by Bioinspired Nonheme Oxoiron(IV) Complexes, Including Hydroxylation of *n*-Butane

Scott T. Kleespies, Williamson N. Oloo, Anusree Mukherjee, and Lawrence Que, Jr.*

Department of Chemistry and Center for Metals in Biocatalysis, University of Minnesota, Minneapolis, Minnesota 55455, United States

Supporting Information

ABSTRACT: The development of efficient and selective hydrocarbon oxidation processes with low environmental impact remains a major challenge of the 21st century because of the strong and apolar nature of the C−H bond. Naturally occurring iron-containing metalloenzymes can, however, selectively functionalize strong C−H bonds on substrates under mild and environmentally benign conditions. The key oxidant in a number of these transformations is postulated to possess an $S = 2$ Fe^{IV}═O unit in a nonheme ligand environment. This oxidant has been trapped and spectroscopically characterized and its reactivity toward C−H bonds demonstrated for several nonheme iron enzyme classes. In order to obtain insight into the structure−activity relationships of these reactive intermediates, over 60 synthetic nonheme $Fe^{IV}(O)$ complexes have been prepared in various laboratories and their reactivities investigated. This Forum Article summarizes the current status of efforts in the characterization of the C−H bond cleavage reactivity of synthetic $Fe^{IV}(O)$ complexes and provides a snapshot of the current understanding of factors that control this reactivity, such as the properties of the supporting ligands and the spin state of the iron center. In addition, new results on the oxidation of strong C−H bonds such as those of cyclohexane and *n*-butane by a putative $S = 2$ synthetic $Fe^{IV}(O)$ species that is generated in situ using dioxygen at ambient conditions are presented.

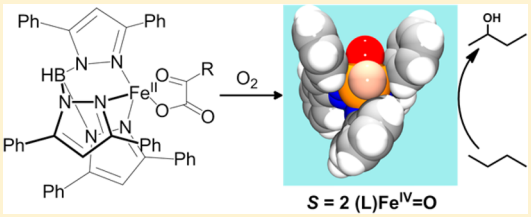

INTRODUCTION

The development of efficient and selective hydrocarbon oxidation processes with low environmental impact remains a major challenge of the 21st century.[1] This is mainly due to a number of factors, which include (i) a large kinetic barrier associated with the C−H bond cleavage step that precedes the functionalization step as a result of the strong (>96 kcal mol^{-1}) and apolar nature of the C−H bonds, (ii) the difficulty in preventing further oxidation of the desired product because its C−H bonds are more activated than those of the hydrocarbon substrate, and (iii) the problem of controlling site selectivity because most organic molecules contain different C−H bonds of comparable strengths. Therefore, not only do new methodologies to cleave the strong C−H bonds of hydrocarbon substrates need to be identified, but these transformations must also occur selectively and under mild, atom-economical, and environmentally friendly conditions.[1−3]

Nature has used metalloenzymes for the selective functionalization of strong C−H bonds on substrates such as alkanes, fatty acids, and steroids in atom-economical transformations that operate under mild and environmentally benign conditions.[4,5] These metal-containing enzymes reductively activate molecular oxygen to generate a high-valent oxidant that attacks substrates with excellent regio-, chemo-, and stereoselectivity.[6] In the past 25 years, significant mechanistic insights into how metalloenzymes work have been obtained via the characterization of intermediates by X-ray crystallography and various spectroscopic methods, detailed kinetic studies, synthetic modeling, and computational investigations. Such studies have produced candidates for the active oxidants in several classes of important iron oxygenase enzymes, some of which will be discussed in this Forum Article.

Gaining an understanding of the structure−function relationships in the metalloenzymes not only will be of great interest in its own right but also may aid in the development of selective and efficient synthetic transformations that operate via the biological mechanism.[7] Such "bioinspired" or "biomimetic" catalysts[3,8] may also possess added advantages over the biological systems, such as an expanded substrate scope, increased scale of production, and tunable selectivity and/or specificity. Indeed, recent advances in the trapping and characterization of high-valent oxoiron(IV) complexes have shed light on the fundamental reaction steps and the nature of reactive intermediates in C−H bond cleavage reactions mediated by various metalloenzymes. In this Forum Article, some highlights will be discussed.

C−H Bond Oxygenation by Nonheme Iron Metalloenzymes and Model Complexes. Various iron-containing metalloenzymes reductively activate dioxygen to oxidize strong aliphatic C−H bonds. Cytochrome P450 does so with good regio- and stereoselectivity,[4] and much is known about its

Special Issue: Small Molecule Activation: From Biological Principles to Energy Applications

Received: November 24, 2014
Published: March 9, 2015

DOI: 10.1021/ic502786y
Inorg. Chem. 2015, 54, 5053−5064

Scheme 1. Reactive Iron Enzyme Intermediates That Have Been Spectroscopically Characterized

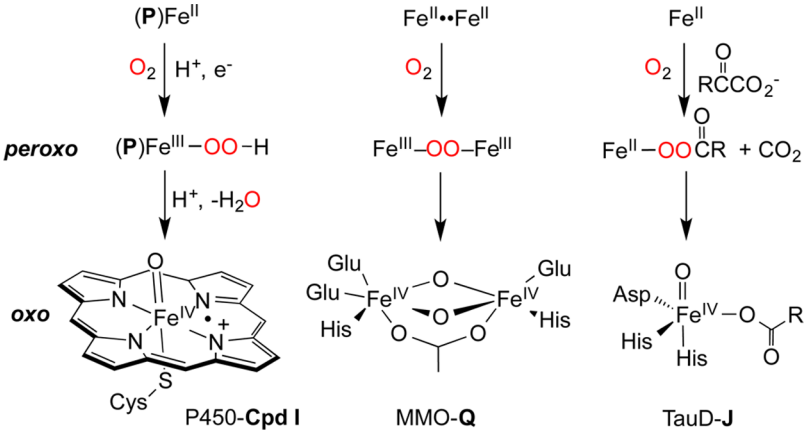

catalytic mechanism.[9−11] This enzyme family binds dioxygen at an active site consisting of an iron(II) porphyrin cofactor that is attached to the protein backbone through an axial cysteine.[12] The bound dioxygen is reduced in one-electron steps to superoxo and peroxo forms and then converted with the help of protons to a (Porph$^{\bullet+}$)Fe^{IV}(O) intermediate called **Cpd I** (Scheme 1), which has been trapped, characterized spectroscopically, and shown to be responsible for substrate oxidation.[13]

Nonheme diiron enzymes such as soluble methane monooxygenase (MMO) and fatty acid desaturases, on the other hand, employ an active site where two iron centers work hand in hand to reductively activate dioxygen and carry out a variety of C−H bond oxidation reactions.[5] Soluble MMO, which is the most studied nonheme diiron oxygenase to date, activates dioxygen at a carboxylate-rich diiron center.[14−16] Following the heme paradigm (Scheme 1), binding of dioxygen onto the diiron(II) center affords a (μ-1,2-peroxo)diiron(III) intermediate called **P**, which has been characterized and shown to epoxidize electron-rich olefins.[17] However, substrate C−H bond cleavage requires a subsequent intermediate called **Q**, which arises from O−O bond cleavage of **P**. Intermediate **Q** has been characterized spectroscopically to have a [Fe$^{IV}_2$(μ-O)$_2$] diamond core[18,19] and demonstrated to be kinetically competent at hydroxylating methane.[20]

Oxoiron(IV) species have also been found to be key oxidizing intermediates in the mechanisms of mononuclear nonheme iron enzymes that catalyze a variety of oxidative transformations, including hydroxylation, halogenation, desaturation, and heterocylic ring formation.[5,21] Dioxygen activation in these enzymes takes place at an iron center that is bound to a 2-His-1-carboxylate facial triad motif.[22] The two electrons required for dioxygen activation are supplied either by organic cofactors like α-ketoglutarate (α-KG),[21] tetrahydrobiopterin,[23] and ascorbate[24,25] or by the substrates themselves (e.g., isopenicillin N synthase).[26−28] The reductive activation of the bound dioxygen leads to the formation of an S = 2 oxoiron(IV) species,[29] which has been trapped and characterized by various spectroscopic methods in several enzyme classes including taurine:α-KG dioxygenase (TauD),[30−32] prolyl-4-hydroxylase (P4H),[33] the halogenases CytC3[34,35] and SyrB2,[36] and pterin-dependent phenylalanine (PheH)[37] and tyrosine hydroxylase (TyrH).[38] The kinetic competence of the oxoiron(IV) intermediates toward C−H bond cleavage has also been demonstrated via large substrate deuterium KIEs.[31] In the cases of TauD, P4H, CytC3, and SyrB2, the oxoiron(IV) intermediates are generated upon oxidative decarboxylation of the α-KG cofactor, as shown in Scheme 1.[29]

Given the identification of oxoiron(IV) species as key intermediates in the catalytic cycles of nonheme iron enzymes,[29] synthetic Fe^{IV}=O complexes have been prepared and their reactivities toward C−H bond cleavage investigated. These efforts have led to the characterization of over 60 synthetic nonheme oxoiron(IV) complexes over the past decade.[39−42] Besides the structural and spectroscopic characterization of these complexes, a wealth of reactivity data involving hydrogen-atom abstraction has rapidly accumulated. This Forum Article summarizes the current status of efforts in the characterization of the hydrogen-atom-transfer (HAT) reactivity of oxoiron(IV) complexes and what factors may control this reactivity. In addition, new results are presented on a model system that activates dioxygen under ambient conditions to generate a putative S = 2 Fe^{IV}(O) species that can oxidize strong C−H bonds such as those of cyclohexane (bond dissociation energy BDE = 99 kcal mol^{-1}) and light alkanes such as n-butane (BDE = 98 and 101 kcal mol^{-1}).[43]

Mechanistic Considerations. Following precedents from studies of high-valent heme complexes,[11,13,44,45] the mechanism of C−H bond oxidation by nonheme Fe^{IV}(O) complexes can be construed to involve at least two steps.[46,47] The first step involves HAT from the target C−H bond to (L)Fe^{IV}(O) to afford an alkyl radical and Fe^{III}OH (Scheme 2). That HAT contributes to the rate-determining step is usually deduced by measuring the kinetic isotope effect (KIE) between protio and deutero substrates and/or demonstrating a linear correlation of

Scheme 2. Proposed Mechanism of C−H Bond Oxidation by Fe^{IV}(O) Complexes[a]

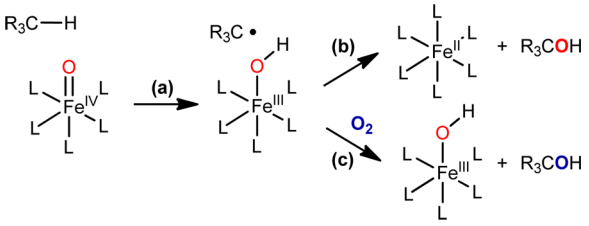

[a]Step a represents HAT, which may be followed by an intramolecular oxygen rebound step b or intermolecular trapping of the alkyl radical with traps such as dioxygen (step c).

DOI: 10.1021/ic502786y
Inorg. Chem. 2015, 54, 5053−5064

the reaction rate constants on substrate C−H BDEs, based upon the Evans−Polanyi relationship of $\log(k_H) = \alpha\Delta H^\circ$ + constant. ΔH° is directly related to the strength of the C−H bond, while the proportionality constant α is a measure of how far the transition state has progressed along the reaction coordinate.[48,49]

Insights into HAT from the target C−H bond to an $Fe^{IV}(O)$ moiety have been obtained from the application of density functional theory (DFT).[50−55] In a tetragonal $Fe^{IV}(O)$ geometry, the key frontier molecular orbitals (FMOs) likely to be involved in the HAT step are the singly occupied π^* $d_{xz/yz}$ and the unoccupied σ^* d_{z^2} orbitals (Figure 1). The transfer of a

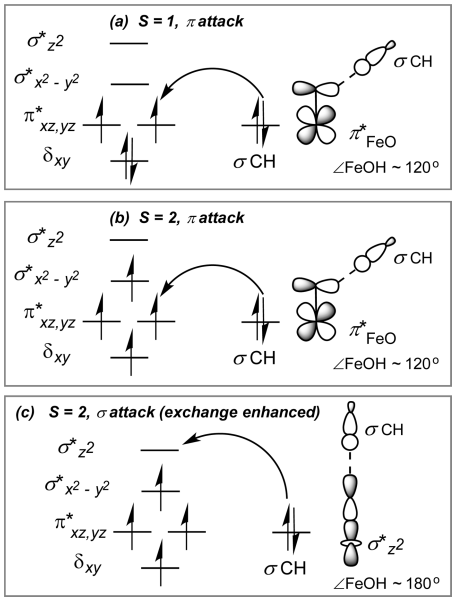

Figure 1. (a) C−H abstraction by $S = 1$ Fe^{IV}═O complexes via the π-attack pathway. C−H abstraction by $S = 2$ Fe^{IV}═O complexes (b) via the π-attack pathway and (c) via the σ-attack pathway. Adapted with permission from ref 51. Copyright 2011 Nature Publishing Group.

hydrogen atom from the σ(C−H) orbital to the $Fe^{IV}(O)$ species results in protonation of the oxo atom and the introduction of an electron into one of the singly occupied π^* $d_{xz/yz}$ orbitals of Fe═O. Because of the shape of the π^* FMO, this "π-attack" pathway requires a nearly perpendicular approach of the substrate C−H bond relative to the Fe═O bond with a Fe−O−HC angle of ∼120° for optimal overlap with the oxo $p_{x/y}$ orbital (Figure 1a,b).[50,55] Such an approach could result in substantial steric interactions between the substrate and equatorial ligands that may raise the reaction barrier for the π-attack pathway.

An additional reaction pathway available only to $S = 2$ Fe^{IV}═O complexes involves the unoccupied Fe═O $\sigma^*d_{z^2}$ orbital, which requires a vertical approach of the C−H σ-bond collinear with the Fe═O bond for an Fe−O−HC angle of 180° for optimal orbital overlap (Figure 1c).[50,55] Such a vertical substrate attack would minimize steric interactions with the equatorial ligands during the C−H abstraction process. Furthermore, the transfer of an electron into the empty d_{z^2} orbital results in a large increase in the number of exchange interactions, which lowers the quintet barrier relative to its triplet counterpart.[51] These two factors have been proposed to make a high-spin $S = 2$ complex more reactive than the corresponding intermediate-spin $S = 1$ species.[51,52,55]

The higher reactivity of the $S = 2$ state has been exploited by Shaik in the two-state-reactivity (TSR) model that was put forward to rationalize the reactivity differences among various $S = 1$ $Fe^{IV}(O)$ complexes.[53,56] This model postulates that the net activation barrier for C−H bond cleavage by intermediate-spin oxoiron(IV) complexes represents a weighted blend of the barrier on the ground triplet and excited quintet surfaces. Given that the transition state on the quintet surface lies lower than that on the triplet ground state,[51] decreasing the triplet−quintet gap (ΔE_{TQ}) increases the accessibility of the quintet state, which, in turn, lowers the net barrier for C−H cleavage (Figure 2). Thus, ligand-field effects that decrease ΔE_{TQ} are predicted to increase the rate of C−H bond cleavage by $S = 1$ $Fe^{IV}(O)$ complexes.

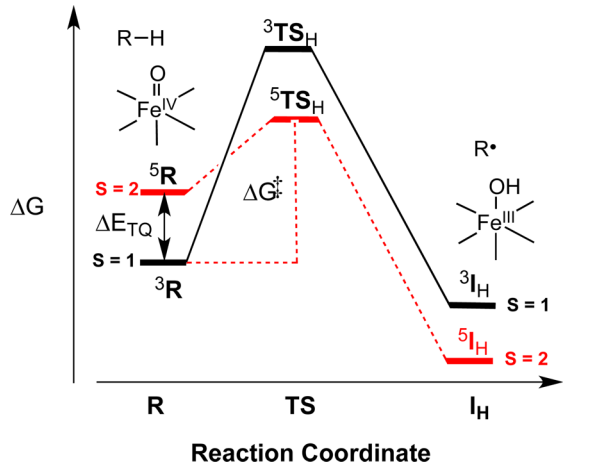

Figure 2. Representation of the TSR scenario during the hydrogen-atom-abstraction reactions of an $Fe^{IV}(O)$ complex in a tetragonal geometry. ΔE_{TQ} is the energy gap between the triplet and quintet states, $^{3,5}TS_H$ are the respective transition states. $\Delta G^{\ddagger}$ is the free-energy barrier from the ground state ^3R to ^5TS_H, and $^{3,5}I_H$ are the corresponding hydrogen-atom-abstracted intermediate complexes. Adapted with permission from ref 57. Copyright 2015 Amercian Chemical Society.

Table 1 compares HAT reactivity data for selected oxoiron(IV) complexes characterized to date. A quick perusal shows that the oxidation rates for 9,10-dihydroanthracene (DHA) reported at −30 or −40 °C can differ by as much as 6 orders of magnitude (Figure 3a). Although the number of examples is smaller, cyclohexane oxidation rates also span a comparable range when the 65 °C temperature difference of the reactions is taken into account (Figure 3b). It is clear from Table 1 and Figure 3 that the HAT reactivity of nonheme $Fe^{IV}(O)$ complexes can be markedly affected by the properties of the supporting ligands such as topology, denticity, and sterics, as well as the nature of the variable cis or trans ligand and the spin state of the iron center. These factors will be discussed in the following sections.

***S* = 1 Oxoiron(IV) Complexes.** Our discussion starts with oxoiron(IV) complexes supported by an equatorial array of four nitrogen donors, which leaves a site available trans to the oxo ligand for coordination by a monodentate ligand such as the solvent or added anions (Scheme 3). The prototypical example for this group is the $S = 1$ $[(TMC)Fe^{IV}(O)(NCMe)]^{2+}$ complex **1**, which was prepared by the oxidation of its iron(II) precursor with iodosylbenzene (PhIO) in CH_3CN at −40 °C.[59] Complex **1** was the first oxoiron(IV) complex to be isolated

DOI: 10.1021/ic502786y
Inorg. Chem. 2015, 54, 5053−5064

Table 1. C−H Bond Cleavage Reactivity of Various Oxoiron(IV) Complexes

entry	(L)Fe^{IV}(O) where L =	λ_{max}/nm (ε/M^{-1} cm^{-1})	δ (ΔE_Q/mm s^{-1})	DHA (77*)	CHD (78*)	PhEt (87*)	c-C_6H_{12} (99*)	temp (°C)	ref
1	TMC	824 (400)	0.17 (1.24)			9.6×10^{-5}		15	58
				0.14	0.12			0	59, 60
				2.5×10^{-3}	6.4×10^{-4}			−40	61
2	TBC	885 (360)	0.22 (0.97)			0.015		15	58
3	13-TMC	735 (240)	0.12 (1.98)	5.7	5.4			−40	61
4	N4Py	695 (400)	−0.04 (0.93)	18		4.0×10^{-3}	5.5×10^{-5}	25	46, 62
						1.3×10^{-3}		15	58
					0.07			−40	62
5	Bn-TPEN	740 (400)	0.01 (0.87)	100		0.069	3.9×10^{-4}	25	46, 62
					0.96			−40	62
6	TPA[a]	724 (300)	0.01 (0.92)	4.8		5.4×10^{-3}		−30	64, 65
7a	PyTACN	750 (200)	0.05 (0.73)				4.0×10^{-4}	25	66
				5.7	4.2	0.016[b]		15	66
				0.81				−30	67
7b	Py_2TACN	740 (340)		7.4				25	62
		900 (200)			0.027			−40	
8*α*	*cis*-*α*-BQCN	758 (120)				0.16		0	68
8*β*	*cis*-*β*-BQCN	770 (180)				0.014		0	68
9a	BP1	760 (130)		8				−35	69
9b	BP2	730 (400), 916 (sh)		1.1				25	62
					0.37			−40	
9c	BP3	730 (380), 896 (sh)		40				25	62
					0.014			−40	
11	Me_3NTB	770 (200)	0.02 (1.53)	3.1×10^3	9.4×10^2	1.5	0.25	−40	63
15	TMG_3tren	400 (9800)	0.09 (−0.29)	9.0×10^{-2}	1.2			−30	70
		825 (260)							
17	tpa^{Ph}	400, 900	0.09 (0.51)		1.4			−30	84
18	TMG_2dien	380 (8200)	0.08 (0.58)	57	18			−30	71
		805 (270)							
19	TQA	650 (300)	0.24 (−1.05)			2.1	0.37	−40	72
		900 (75)							

*The value in parentheses reflects the C−H bond dissociation energy of this substrate in units of kcal mol^{-1}. [a]Although spectroscopic characterization was conducted on $[(TPA)Fe^{IV}(O)]^{2+}$, the kinetic data were obtained using $[(5Me_3TPA)Fe^{IV}(O)]^{2+}$. The electronic absorption spectra for the $(5Me_3TPA)Fe^{IV}(O)$ and $(TPA)Fe^{IV}(O)$ complexes at −40 °C are similar. [b]The oxidation rate for PhEt is not available; listed instead is that for 2,3-dimethylbutene (BDE = 84 kcal mol^{-1}).

and crystallographically characterized. All four methyl groups of the TMC ligand were found to be on the same side of the macrocycle and opposite to the position of the oxo group, and MeCN occupied the coordination site trans to the oxo group. This complex exhibits a $t_{1/2}$ of 10 h at 25 °C. Two other closely related complexes have also been crystallized, namely, $[(TMC_{PY})Fe^{IV}(O)]^{2+}$ and $[(TMC_{DMA})Fe^{IV}(O)]^{2+}$ (Scheme 3),[73] where one of the hydrogen atoms on a methyl group in each complex was respectively replaced by a pyridyl group and a $-C(O)NMe_2$ group, providing a fifth ligand that coordinated to the iron center trans to the oxo group. The pyridine substitution decreased $t_{1/2}$ of the complex to 7 h, while the amide substitution increased $t_{1/2}$ of the complex 12-fold to 120 h, demonstrating the importance of the axial ligand in modulating the stability of the Fe^{IV}=O complex.

The high thermal stability of these complexes translated into a relatively poor C−H abstraction reactivity,[59] and only substrates with relatively weak C−H bonds could be oxidized.[60,61] Within this narrow range of substrates, a linear relationship could be discerned in the plot of log k_2' values versus substrate C−H BDE values for $[(TMC)Fe^{IV}(O)(NCMe)]^{2+}$, with faster rates associated with weaker C−H bonds. These results indicated the involvement of a rate-determining C−H abstraction step, which was supported by the observation of nonclassical KIE values of 10−20 for dihydroanthracene and xanthene oxidation.[60,61]

Substitution of the axially bound MeCN of $[(TMC)Fe^{IV}(O)(NCMe)]^{2+}$ with anions to obtain an $[(TMC)Fe^{IV}(O)(X)]^+$ ($\mathbf{1_X}$) series shortened their $t_{1/2}$ values and accelerated the oxidation of DHA (BDE = 77 kcal mol^{-1}) and cyclohexadiene (CHD; BDE = 78 kcal mol^{-1}). The HAT rates increased with the basicity of the anionic ligand X^- (X = NCMe < O_2CCF_3 < N_3 < SR),[60] spanning a 40-fold difference in the HAT reactivity and exhibiting a linear correlation when log k_2 was plotted against the redox potential of $\mathbf{1_X}$ (see the black line in Figure 4: black crosses for DHA and filled diamonds for CHD). This observed trend was surprising because the oxidizing power of the oxoiron(IV) center would be expected to diminish as the axial ligand became more electron-donating. The counter-intuitive trend was rationalized by invoking the TSR model discussed in the Introduction (Figure 2).[56,60] DFT calculations showed that the energy gap between the ground triplet and excited quintet states (ΔE_{TQ}) decreased as the axial ligand became more electron-donating. The decreased separation between these two states increased the accessibility to the more reactive quintet state as the hydrogen-atom abstraction progressed along the reaction coordinate, thereby resulting in the experimentally observed "antielectrophilic" trend. In

DOI: 10.1021/ic502786y
Inorg. Chem. 2015, 54, 5053−5064

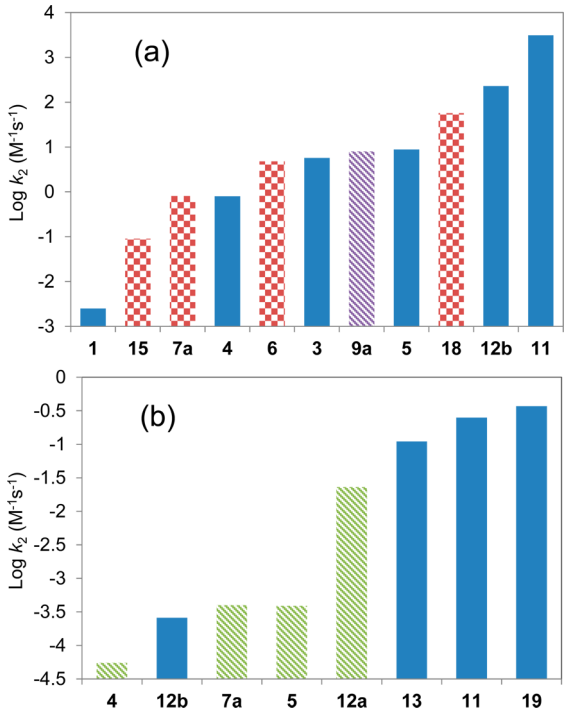

Figure 3. Reactivity comparisons of high-valent oxoiron complexes in the oxidation of (a) DHA at −30 °C (checkered red), −35 °C (striped purple), and −40 °C (solid blue) and (b) cyclohexane at 25 °C (striped green) and −40 °C (solid blue). See Schemes 3−6 for structures of the respective (L)Fe^{IV}(O) complexes.

Scheme 3. S = 1 Fe^{IV}(O)(L) Complexes Supported by Cyclam and Related Ligands

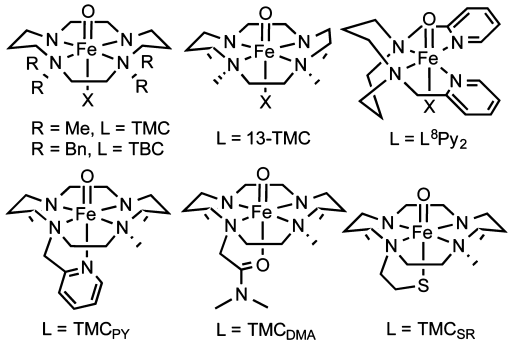

contrast, the oxygen-atom-transfer (OAT) rates for the series (represented by green filled and open circles in Figure 4) followed the opposite but expected trend, where more electrophilic Fe^{IV}=O complexes reacted more rapidly with PPh_3 (Figure 4, red line).

When the $\mathbf{1}_X$ series was expanded to include subsequently characterized $[(TMC_{PY})Fe^{IV}(O)]^{2+}$, $[(TMC_{DMA})Fe^{IV}(O)]^{2+}$, and the conjugate base of $[(TMC_{DMA})Fe^{IV}(O)]^{2+}$,[73] one linear correlation held up but the other did not. The additional PPh_3 data points (Figure 4, green open circles) conformed to the red OAT line, supporting the correlation between the OAT rates and the electrophilicity of the Fe=O unit. However, the corresponding data points for CHD oxidation (Figure 4, red open diamonds) did not fall at all near the black antielectrophilic line, suggesting that there are other factors besides the redox potential that control the HAT reactivity. More recent DFT calculations suggested that the HAT data for

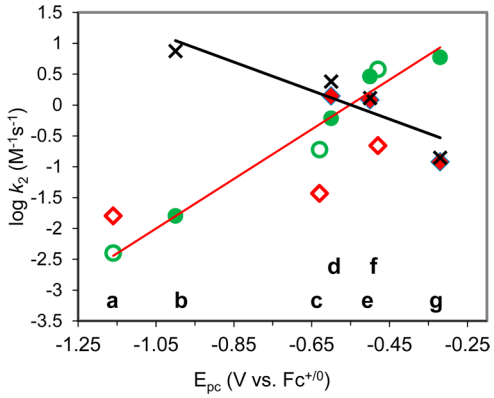

Figure 4. Plot of log k_2 determined in the oxidation of CHD (red diamonds), DHA (black crosses), and PPh_3 (green circles) at 0 °C against $E_{p,c}$ values of $[Fe^{IV}(O)(TMC)(X)]^{n+}$ complexes in CH_3CN or 1:1 CH_3CN/CH_3OH. The filled circles, filled diamonds, and crosses represent data reported in ref 60, while the open circles and open diamonds correspond to more recent data reported in ref 73. The red line is the linear correlation for the OAT rates represented by the filled and open circles, and the black line is the linear correlation for the HAT rates represented by the filled diamonds and crosses. The letters at the bottom of the figure correspond to the axial ligands of **1**, with **a** = −CH=C(O$^-$)(NMe$_2$), **b** = RS$^-$, **c** = −CH$_2$C(O)NMe$_2$, **d** = N_3^-, **e** = CF_3COO^-, **f** = −CH$_2$Py, and **g** = MeCN. See Scheme 3 for structures of the Fe^{IV}(O) complexes.

the newer complexes could be rationalized by including tunneling contributions.[57]

Variations on the TMC macrocycle have also been investigated. Replacing the *N*-methyl substituents of the TMC ligand with benzyl groups to give the S = 1 $[(TBC)Fe^{IV}(O)]^{2+}$ complex **2** resulted in a 150-fold increase in the HAT reactivity (ethylbenzene oxidation),[58] which could be rationalized by a TSR argument. The weaker ligand field, as indicated by the red shift of its near-IR band to 885 nm, presumably increased accessibility to the more reactive quintet spin state. Shrinking the TMC macrocycle by one carbon atom to obtain the smaller 13-TMC analogue **3** also increased the HAT reactivity (DHA oxidation) but by 3 orders of magnitude.[61] However, in this case, the near-IR band blue-shifted to 735 nm, so the TSR argument cannot be applied to this case. These contradictory observations demonstrate that understanding the HAT reactivity is not so straightforward.

The second Fe^{IV}=O complex to be crystallized was supported by the pentadentate N4Py ligand.[46,74] $[(N4Py)Fe^{IV}(O)]^{2+}$ (**4**) is another S = 1 complex and has $t_{1/2}$ of 60 h (Scheme 4). Despite the fact that this complex was 6-fold more stable than **1** at 25 °C, **4** was found to attack a much broader range of hydrocarbon substrates. Indeed, it was the first nonheme Fe^{IV}=O complex shown to cleave the C−H bonds of cyclohexane (BDE = 99 kcal mol^{-1}), albeit quite slowly. The substitution of N4Py with Bn-TPEN, a pentadentate ligand with a different topology, gave rise to the less stable Fe^{IV}=O complex **5** ($t_{1/2}$ = 3 h at 25 °C), which was more reactive and oxidized cyclohexane at a 10-fold faster rate.

Additional complexes of pentadentate ligands with various combinations of tertiary amine and pyridine donors, namely, Py_2TACN (**7b**), BP2 (**9b**), and BP3 (**9c**) (Scheme 4) behaved similarly, with higher reactivity associated with complexes exhibiting higher redox potentials and having pyridine rings perpendicular to the Fe=O unit.[62] An excellent positive correlation was observed for the plot of log k_2(OAT) values

DOI: 10.1021/ic502786y
Inorg. Chem. 2015, 54, 5053−5064

Scheme 4. S = 1 $Fe^{IV}(O)(L)$ Complexes Supported by Pentadentate and Tetradentate Ligands

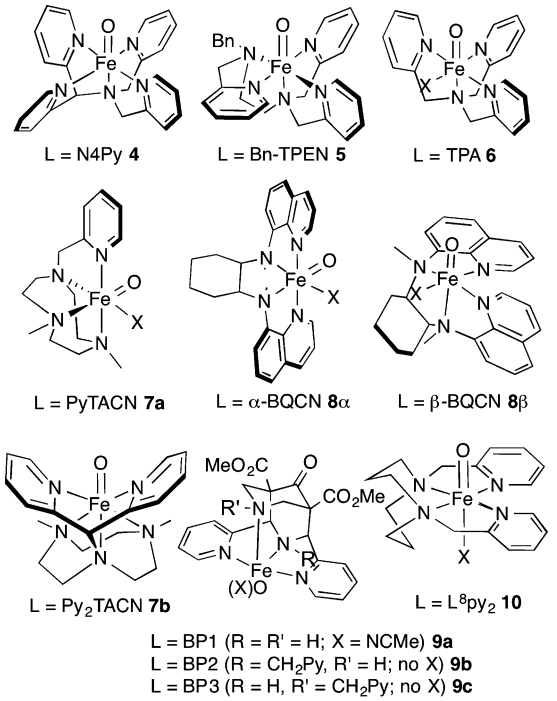

versus $Fe^{IV/III}$ potentials, where the OAT rates increased with higher Fe=O electrophilicity. In contrast to the antielectrophilic trend observed for the $\mathbf{1}_X$ series (Figure 4, black line), the HAT rates parallel the electrophilic trend observed in the plot of log k_2(OAT) versus $Fe^{IV/III}$ potential, although the correlation is not as good as that found for the OAT rates. It was suggested that the downshift in the rates seen for the BP2/BP3 subset may be associated with constraints imposed by the bicyclic framework of the BP ligands.

For **4** and **5**, large nonclassical KIE values of 30 and 50, respectively, were observed at 25 °C in the oxidation of ethylbenzene versus ethylbenzene-d_{10}; in fact, for **5**, the KIE value was temperature-dependent and increased from 40 at 40 °C to 400 at −40 °C, which was ascribed to hydrogen-atom tunneling effects.[75] Further investigation of the KIE value as a function of the substrate revealed a surprising pattern of reactivity, where nonclassical values were found for substrates with C−H BDE values of up to 93 kcal mol^{-1}, but classical values were associated with substrates with stronger C−H bonds. For example, a KIE value of 6 was obtained for cyclohexane oxidation by **5** at 40 °C. This unexpected behavior was rationalized via the TSR model, where the tunneling mechanism depends on the C−H BDE.

Closely related Fe^{IV}=O complexes supported by tetradentate ligands have also been found to have S = 1 ground states. There are fewer systematic studies that allow convenient comparison of the HAT reactivity, but it seems likely that oxoiron(IV) complexes of tetradentate ligands are more reactive than their pentadentate counterparts (Figure 3 and Table 1). The two $[(BQCN)Fe^{IV}(O)(NCMe)]^{2+}$ complexes **8*α*** and **8*β*** represent an interesting pair because they are topological isomers (Scheme 4).[68] **8*α*** was found to oxidize ethylbenzene by a factor of 10 faster than **8*β***, demonstrating the role that ligand topology can play in modulating the HAT reactivity. This reactivity difference may stem from a difference in the $Fe^{IV/III}$ redox potential, with that of **8*α*** (0.72 V vs SCE) being 0.11 V higher than that of **8*β*** (0.61 V vs SCE).

A study was also carried out with a series of $[(L^8py_2)Fe^{IV}(O)(L)]^{2+}$ (**10**; Scheme 4) complexes, where the supporting L^8py_2 ligand provided an equatorial array of four nitrogen donors and L represented an axial pyridine *N*-oxide donor with various 4-substituents.[76] In the set of HAT experiments with benzyl alcohol as the substrate, the oxidation rates accelerated with more electron-donating substituents, corresponding to a Hammett ρ value of −1.4, consistent with the antielectrophilic trend found for HAT reactions of the $\mathbf{1}_X$ series (Figure 4, black line). Surprisingly, the corresponding OAT reactions also exhibited an antielectrophilic trend with a Hammett ρ value of −1.3, which was quite a puzzling observation.

The complex that stands out among its peers in the S = 1 Fe^{IV}=O subset is $[(Me_3NTB)Fe^{IV}(O)]^{2+}$ (**11**; Scheme 5)

Scheme 5. Highly Reactive High-Valent Oxoiron Complexes

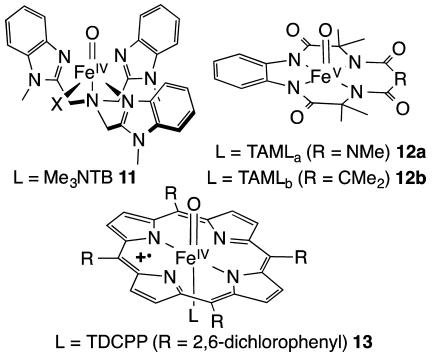

because it exhibits the highest oxidation rate of cyclohexane (BDE = 99 kcal mol^{-1}) to date for any S = 1 Fe^{IV}=O complex (Figure 3).[63] The cyclohexane oxidation ability of **11** even exceeds those of the two $[(TAML)Fe^{V}(O)]^{-}$ complexes **12a** and **12b**[77,78] and $[(TDCPP^{\bullet})Fe^{IV}(O)]^{+}$ (**13**),[63] which is a synthetic analogue of **Cpd 1**, the highly reactive intermediate involved in the oxidation chemistry of heme enzymes. The HAT reactivity of **11** is at least 3 orders of magnitude higher than that of **6**, and the main structural difference between the two is that **11** has three benzimidazole donors instead of pyridines. The bar graphs in Figure 3 emphasize that the S = 1 complexes shown have DHA oxidation rates covering a range of 6 orders of magnitude, while the subset that can oxidize cyclohexane exhibits rates that span a similar range after adjustment for temperature differences.

S = 2 Oxoiron(IV) Complexes. The majority of the Fe^{IV}=O units found in synthetic nonheme complexes described thus far have S = 1 ground states, while those associated with nonheme iron enzyme intermediates have S = 2 ground states. Calculations have predicted S = 2 Fe^{IV}=O units to be much more reactive toward C−H abstraction than their S = 1 counterparts.[50−56,79] However, the paucity of synthetic examples of S = 2 oxoiron(IV) complexes makes it difficult to ascertain experimentally this computational prediction.

The first example of a synthetic S = 2 Fe^{IV}=O complex was reported by Bakac and co-workers,[80,81] which was generated by the ozonolysis of an aqueous $[Fe^{II}(OH_2)_6]^{2+}$ ion at 25 °C and formulated as $[(H_2O)_5Fe^{IV}(O)]^{2+}$ (**14**). This complex exhibited a half-life of only 20 s at room temperature and was found to attack substrates like CH_3CN with very high rate constants.

DOI: 10.1021/ic502786y
Inorg. Chem. 2015, 54, 5053−5064

However, its high HAT reactivity, together with the fact that it could only be observed in aqueous media, made this complex a challenge to characterize with the spectroscopic detail achieved for other Fe^{IV}=O complexes.

The first S = 2 Fe^{IV}(O) complex to be isolated was the trigonal-bipyramidal $[(TMG_3tren)Fe^{IV}(O)]^{2+}$ complex **15** (Scheme 6).[70] The C_3 symmetry about the iron(IV) center

Scheme 6. Crystallographically and/or Spectroscopically Characterized S = 2 Fe^{IV}(O)(L) Complexes

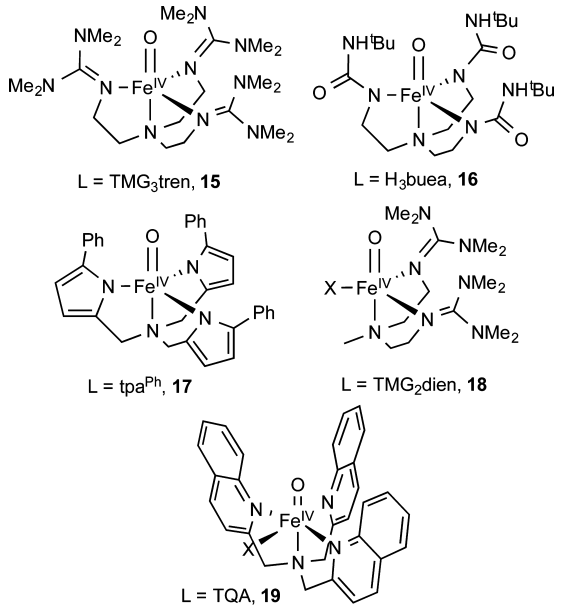

gave rise to a d-orbital splitting pattern with a $(d_{xz},d_{yz})^2(d_{xy},d_{x^2-y^2})^2(d_{z^2})^0$ configuration. Although this complex had a $t_{1/2}$ value at 25 °C of 30 s, just slightly longer than that of **14**, the possibility of cooling the MeCN solvent to −40 °C allowed its half-life to be extended significantly. In addition, it was determined that its self-decay occurred by intramolecular attack of a ligand methyl C−H bond by the Fe=O unit, showing that this Fe=O moiety was capable of attacking a relatively strong C−H bond (BDE ∼ 93 kcal mol^{-1}). On the basis of this result, the 12 ligand methyl groups were perdeuterated in order to further extend the lifetime of **15**, which enabled its characterization by X-ray crystallography.[82] A similar C_3-symmetric ligand design strategy was employed by Borovik et al.[83] and Chang et al.[84] to obtain additional examples of S = 2 Fe^{IV}=O complexes, namely, $[(H_3buea)Fe^{IV}(O)]^-$ (**16**) and $[(tpa^{Ph})Fe^{IV}(O)]^-$ (**17**) (Scheme 6). An X-ray structure was also obtained for the Borovik complex.

The intermolecular HAT reactivity of **15** was, however, quite sluggish because of the near-encapsulation of the Fe=O unit by the bulky tetramethylguanidine groups of the TMG_3tren supporting ligand that hindered substrate access.[82] Its rate of DHA oxidation at −30 °C was, in fact, 20-fold slower than that of **4** (Figure 3), but the corresponding rates of oxidation of the smaller CHD (77 kcal mol^{-1}) were essentially identical, corroborating the steric access argument.[70] The higher reactivity predicted for an S = 2 Fe^{IV}=O moiety was realized when one arm of the TMG_3tren supporting ligand was replaced by a methyl group to obtain a less sterically hindered TMG_2dien ligand (Scheme 6), and the corresponding S = 2 $[(TMG_2dien)Fe^{IV}(O)]^{2+}$ complex (**18**) was found to have a DHA oxidation rate 600-fold faster than that of **15** (Figure 3).[71]

An even more reactive S = 2 complex, $[(TQA)Fe^{IV}(O)(NCMe)]^{2+}$ (**19**), has just been obtained by substituting the pyridine moieties of the TPA ligand of **6** with weaker-field quinoline ligands (Scheme 6).[72] This complex has a half-life of 15 min at −40 °C and is formulated as a six-coordinate complex, unlike the previously discussed S = 2 complexes **15**−**18**. Significantly, **19** exhibits the highest cyclohexane oxidation rate (k_2 = 0.37 M^{-1} s^{-1} at −40 °C) found to date for this class of complexes (Figure 3b). For comparison, the closely related S = 1 $[Fe^{IV}(O)(TPA)(NCMe)]^{2+}$ complex **6** does not react at all with cyclohexane at −40 °C, while the cyclohexane oxidation rates for the S = 1 complexes $[Fe^{IV}(O)(N4Py)]^{2+}$ (**4**) and $[Fe^{IV}(O)(BnTPEN)]^{2+}$ (**5**) at 25 °C are 3−4 orders of magnitude slower than that for **19** at −40 °C even without correcting for the 65 °C temperature difference.[46] The observed reactivity of **19** thus supports the DFT-based expectations of a more reactive S = 2 Fe^{IV}=O center.

An exception to this general trend is the S = 1 complex $[Fe^{IV}(O)(Me_3NTB)]^{2+}$ (**11**), which is almost as reactive as **19**, with k_2(cyclohexane) = 0.23 M^{-1} s^{-1} at −40 °C.[63] This surprising similarity suggests that Fe^{IV}(O) complexes, despite having different ground spin states, can achieve comparably high HAT reactivity. DFT calculations on **11** suggest that its high reactivity derives from a highly reactive S = 2 excited-state surface that lies in close proximity of the S = 1 ground state. If this postulate can be experimentally verified, these results would suggest that oxoiron(IV) complexes in the S = 1 state can be just as reactive as their S = 2 congeners as long as the excited S = 2 spin state is easily accessible. Clearly, more effort is needed to assess the relative energies of the S = 1 and 2 spin states in oxoiron(IV) complexes experimentally and correlate these ΔE_{TQ} values with their observed HAT reactivity.

A challenge in analyzing the above reactivity comparisons is how to factor in the effect of the supporting ligand. In the cases discussed thus far, different supporting ligands with distinct topologies were required to obtain a different spin state for the Fe^{IV}=O unit. Que and co-workers found a way to address this challenge by preparing a series of oxo-bridged diiron complexes (**20**−**25**; Figure 5) supported by the same TPA* ligand [TPA* = tris(3,5-dimethyl-4-methoxypyridyl-2-methyl)amine].[64,85] This series consisted of $Fe^{III}Fe^{IV}$ and $Fe^{IV}Fe^{IV}$ complexes with either an $Fe_2(\mu\text{-O})_2$ diamond core or an Fe−O−Fe=O open core, and for the latter subset, the Fe^{IV}=O unit could have an S = 1 or 2 spin state depending on the oxidation state of the adjacent iron center (Figure 5). Because the reactive members of this series could only be prepared and studied at −80 °C, DHA was the substrate of choice for comparing the C−H bond cleavage ability of this series of complexes. This comparison clearly demonstrates that a terminal oxo is at least 100-fold better at HAT than a bridging one and an S = 2 Fe^{IV}=O unit is 1000−10000-fold faster at HAT than its S = 1 analogue. The most reactive members of this series have measured rates of DHA oxidation of 320−360 M^{-1} s^{-1} at −80 °C,[64,86] which exceeds values obtained at −30 or −40 °C for all complexes shown in Figure 3a except for the S = 1 Me_3NTB complex (**11**). When adjusted for the 40 °C temperature difference, the DHA oxidation rates for **24** and **25** are likely to exceed that of the Me_3NTB complex.[63] These results provide the strongest support to date for the consensus DFT predictions of a more reactive S = 2 Fe^{IV}=O moiety.

DOI: 10.1021/ic502786y
Inorg. Chem. 2015, 54, 5053−5064

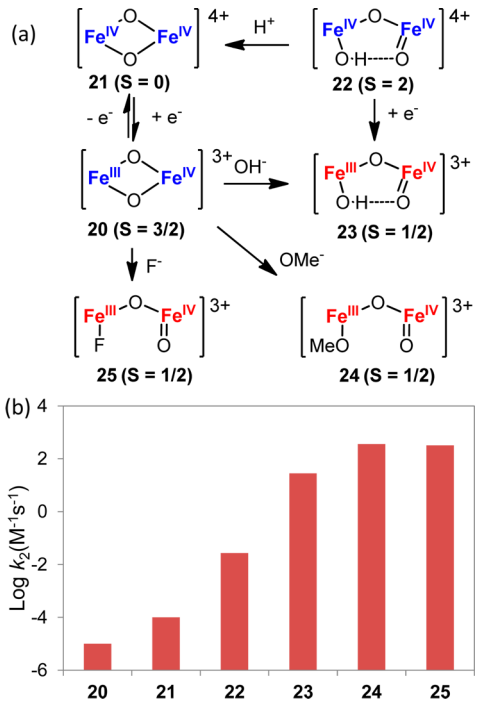

Figure 5. (a) Interconversions among oxo-bridged diiron-TPA* complexes **20**–**25**. Red and blue fonts respectively represent high- and intermediate-spin iron centers. (b) Comparison of DHA oxidation rates of the various diiron-TPA* complexes at −80 °C.

RESULTS AND DISCUSSION

C–H Bond Cleavage by a Fleeting Fe^{IV}=O Species Produced by Dioxygen Activation. All the Fe^{IV}=O complexes described above have been generated by an oxidant other than dioxygen, which has allowed them to accumulate and be characterized with various spectroscopic methods and sometimes by X-ray crystallography. An exception to this pattern is the putative oxoiron(IV) species that is produced by the oxygenation of [Fe^{II}(Tp^{Ph2})(O$_2$CC(O)Ph)] (**26a**), an iron(II) complex that serves as a functional model for α-KG-dependent enzymes like TauD (Scheme 1). Upon exposure to dioxygen in a benzene solvent at room temperature, **26a** undergoes oxidative decarboxylation of its benzoylformate ligand (the α-KG analogue) to form a green chromophore designated as [Fe^{III}(Tp^{Ph2}*)(O$_2$CPh)] (**27a**).[89] The latter has been identified as an iron(III) phenolate complex, resulting from self-hydroxylation of one of the ligand phenyl rings (Figure 6, left). Kinetic studies show that the reaction rate is first-order in the iron complex and first-order in dioxygen, indicating that the rate-determining step corresponds to an early phase of the reaction. By analogy to the α-KG-dependent enzymes, it is proposed that the oxidative decarboxylation step forms a yet unobserved Fe^{IV}=O oxidant **28a**, which DFT calculations suggest to have an S = 2 ground state when the carboxylate is coordinated in a monodentate fashion.[74,88] A space-filling model of the putative oxidant is shown in Figure 6, right.

We previously showed that it was possible to intercept the high-valent species **28a** by introducing external substrates that could be oxidized intermolecularly in competition with the intramolecular ligand hydroxylation.[88] The lower yield of the green chromophoric product from the latter reaction was used as a convenient probe for assessing the relative rates of intermolecular and intramolecular oxidation. Indeed, the addition of 10 equiv of PhSMe into the reaction of **26a** with dioxygen completely prevented intramolecular self-hydroxylation. Instead, a colorless [Fe^{II}(Tp^{Ph2})(O$_2$CPh)(OSR$_2$)] adduct was observed based on electrospray ionization mass spectrometry, NMR, and Mössbauer evidence. The sulfoxide adduct formed in 70% yield, a value comparable to the amount of self-hydroxylated product obtained in the absence of thioanisole.

Probing the thioanisole interception further revealed some interesting but expected insights. The addition of stoichiometric PhSMe suppressed formation of the self-hydroxylated product by 60%, demonstrating the high oxo-transfer ability of the putative Fe^{IV}=O oxidant **28a**. Substituting PhSMe with the more electron-rich tetrahydrothiophene decreased by 90% the amount of self-hydroxylated product, while the less electron-rich Ph$_2$S had the opposite effect (40%). So, **28a** is sensitive to the basicity of the substrate. It should be noted, however, that the reaction time was unchanged for these three experiments because the rate-determining step is associated with the formation of **28a** rather than its decay.

In the 2009 paper on this system, limited success was reported in intercepting **28a** with hydrocarbons.[88] While the addition of substrates with weak C–H bonds such as DHA, fluorene, or cyclohexene significantly decreased the yield of the self-hydroxylated product, potential substrates with stronger C–H bonds were much less effective. Indeed, the addition of 0.1 M ethylbenzene (BDE = 87 kcal mol^{-1}), toluene (BDE = 90 kcal mol^{-1}), or cyclohexane (BDE = 99 kcal mol^{-1}) did not affect the yield of **27a**, raising the possibility that **28a** may not be a powerful enough oxidant to be able to cleave these stronger C–H bonds. However, the observation that the use of 0.1 M cyclooctane (BDE = 95 kcal mol^{-1}) as a substrate slightly

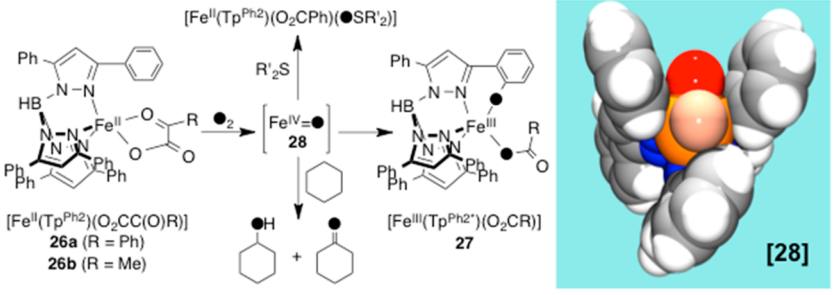

Figure 6. Left: Some reactions of **26a**/**26b** with dioxygen in benzene at 25 °C. Right: DFT-calculated model for the putative oxidant. The peach-colored atom in front is an oxygen atom from the benzoate ligand, and the benzoyl moiety was excised to give a clearer view of the iron center. Adapted with permission from ref 88. Copyright 2009 Wiley-VCH Verlag GmbH & Co. KGaA.

DOI: 10.1021/ic502786y
Inorg. Chem. 2015, 54, 5053–5064

decreased the yield of **27a** provided some incentive to follow up on these earlier observations and obtain the more recent results described below.

In these more recent experiments, we have used higher substrate concentrations in order to increase the intermolecular oxidation rate and enhance the likelihood of intercepting the nascent Fe^{IV}=O oxidant **28a**. Indeed, this expectation has been borne out in the reactions of **26a** with dioxygen in the presence of up to 2 M toluene or cyclohexane (Figure 7, top, and Tables 2 and S1 in the Supporting Information, SI). For example, with 1 M toluene, the yield of **27a** decreased from 64% to 48% concomitant with the formation of PhCHO in 33% yield. Even more significant were the experiments with 1 M cyclohexane, where even less **27a** was formed (34%) and cyclohexane oxidation products were obtained in 44% yield with a 1:3 ratio of cyclohexanol to cyclohexanone. Parallel experiments carried out on the corresponding pyruvate complex [$Fe^{II}(Tp^{Ph2})$-($O_2CC(O)CH_3$)] (**26b**) to serve as a check on the generality of the results obtained for **26a** gave comparable results (Tables 2 and S1 in the SI). In previous work, **26b** was found to react with dioxygen 4-fold more rapidly than **26a** at 25 °C, achieving completion within 15 min (vs 1 h for **26a**), but the amount of self-hydroxylated **27b** obtained was lower.[87] The lower extent of self-hydroxylation for **26b** may reflect a less efficient formation of **28b** relative to that of **28a** or the decay of a higher fraction of **28b** via an alternative unproductive pathway in competition with self-hydroxylation. However, as seen in Figure 7, bottom, and Table 2, oxygenation of **26b** gave rise to intermolecular oxidation products either equal to or higher than **26a**.

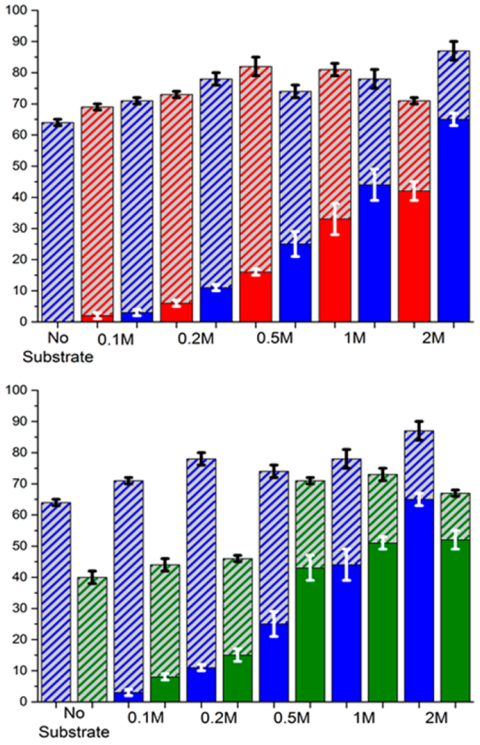

Figure 7. Top: Comparison of the product yields in the reactions of **26a** with dioxygen as a function of the cyclohexane (blue) or toluene (red) concentration. Bottom: Comparison of the product yields in the reactions of **26a** (blue) and **26b** (green) with dioxygen as a function of the cyclohexane concentration. Solid bars: yield of oxidized substrate. Dashed bars: yield of **27a**/**27b**. See Figure 6 for structures of **26a** and **26b**.

Table 2. Product Yields in the Reactions of Dioxygen with $Fe^{II}(Tp^{Ph2})$(BF/PRV) (26a/26b)[a]

		self-hydroxylation yield		substrate oxidation yield	
substrate	concn (M)	**26a**	**26b**	**26a**	**26b**
none		64(1)	40(2)	0	0
toluene	1	48(2)	27(3)	33(5) PKIE = 15	33(3) PKIE = 15
cyclohexane	1	34(3)	22(2)	A + K 44(5), A/K 11/33, PKIE = 12	A + K 51(2), A/K 2/49, PKIE = 12
n-butane	4	39(2)	20(2)	A + K 30(3), A/K 18/12	A + K 39(3), A/K 24/15

[a]Reaction conditions: ~1 mM Fe^{II} complex, 20 °C. Each value is an average of at least three runs. A represents the yield of alcohol. K represents the yield of ketone.

The major (or only) oxidation products observed in the toluene and cyclohexane oxidation are not the alcohols but the corresponding aldehyde or ketone. These outcomes suggest two mechanistic possibilities. The first scenario entails subsequent oxidation of the initially formed alcohol product by a second 1 equiv of **28**. This notion is not implausible because oxygenation of the iron(II) precursor, being rate-determining, makes this step slower than the substrate oxidation step, and alcohol oxidation would be expected to be much more facile than oxidation of the hydrocarbon. The second scenario involves diffusion of the alkyl radical formed in the initial hydrogen-atom abstraction into solution and reaction with the excess dioxygen present. At this point, we are unable to assess the likelihood of the nascent alkyl radical undergoing oxygen rebound. What is clear, however, is that the nascent alkyl radical is formed by the action of a metal-based oxidant, based on results from competitive experiments between a substrate and its perdeuterated analogue in their respective oxidations by **26a** and **26b**. Product analysis showed product KIEs (PKIEs) of 12 for cyclohexane oxidation and 15 for toluene oxidation (Tables 2 and S3 in the SI). Such nonclassical KIE values have been observed for the reactions of C–H bonds with a number of nonheme oxoiron(IV) complexes[61−63,66,72] and support the postulate that **28** is also a member of this class of high-valent iron complexes.

Having demonstrated the ability of **28** to oxidize cyclohexane, we shifted our attention to the light alkane substrate *n*-butane, which has a high solubility in benzene (approximately 4 M at 10 °C by NMR). Indeed, bubbling *n*-butane into a benzene solution of **26a**/**26b**, followed by dioxygen, resulted in a lower yield of **27a**/**27b**, suggesting the interception of **28a**/**28b** by *n*-butane. ^{1}H NMR analysis of the product solution showed the characteristic multiplets of the C2 proton of 2-butanol at 3.7 ppm and the C3 protons of 2-butanone at 1.8 ppm (Figure 8). Because the region below 1.8 ppm contained strong signals from residual *n*-butane, 1D-TOCSY experiments were carried out to identify protons coupled to these multiplets as a means of corroborating our assignments. Indeed, features were observed at 1.5, 1.2, and 0.8 ppm upon irradiation of the 3.7 ppm multiplet belonging to 2-butanol (Figure S3 in the SI) and at 1.6 and 0.8 ppm in the corresponding experiment for the 2-butanone multiplet at 1.8 ppm (Figure S4 in the SI). It

DOI: 10.1021/ic502786y
Inorg. Chem. 2015, 54, 5053−5064

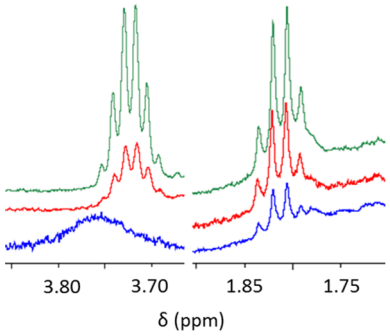

Figure 8. Left: Stacked NMR spectra showing the $CH_3CH_2C(H)OHCH_3$ (3.7 ppm) peak in a reaction solution of **26a** under various conditions. Bottom/blue: Oxidation reaction with *n*-butane as the substrate. Middle/red: Reaction mixture upon the addition of 25 μL of DMSO-d_6 and 2 μL of AcOD-d_4 (0.18 mM/Fe). Top/green: Reaction mixture from the middle spiked with 2-butanol (0.49 mM/Fe). Right: NMR spectra showing the changes in the intensity of the $CH_3C(H_2)COCH_3$ (1.8 ppm) peak upon the addition of 2-butanone to a reaction solution of **26a**. Bottom/blue: Oxidation reaction with *n*-butane as the substrate (0.12 mM/Fe). Middle/red: Solution in blue spiked with 2-butanone (0.36 mM/Fe). Top/green: Solution in red spiked with additional 2-butanone (0.70 mM/Fe).

should be noted that the signal from the C2 proton of 2-butanol in the reaction mixture was broad and lacked resolution, which was similar to the spectrum observed for 2-butanol alone in benzene (Figure S5 in the SI). As shown in Figure 8, left, the addition of small amounts of dimethyl sulfoxide (DMSO) and acetic acid (AcOH) into the reaction mixture substantially sharpened the C2 proton peak and shifted it upfield. We attribute the broadness of the 2-butanol C2−H signal to a hydrogen-bonded cluster of the alcohol in the nonpolar benzene solvent, which was disrupted upon the addition of DMSO and AcOH. Integration of the signals relative to an added tetrachloroethane standard revealed that 2-butanol and 2-butanone were formed in respective yields of 18 and 12% for the reaction with **26a** and 24 and 15% for the reaction with **26b**. In both cases, the addition of aliquots of either 2-butanol or 2-butanone increased the intensities of the 3.7 and 1.8 ppm peaks, as expected (Figures 8 and S6 in the SI). No evidence was found in the NMR spectra for any product arising from C1 oxidation.

Oxidation of *n*-butane by **28** represents the only system thus far to mediate the nonradical oxidation of a gaseous alkane by a high-valent iron oxidant generated from dioxygen. However, there are two other nonheme iron-based systems that carry out similar chemistry on gaseous alkanes, but with ^{t}BuOOH or Oxone as the source of oxidizing equivalents.[89,90] These are promising steps toward the functionalization of gaseous alkanes, but more work is needed to ascertain the nature of the high-valent iron oxidants implicated in these oxidations.

CONCLUSION

In the first part of this Forum Article, we reviewed the C−H bond cleavage abilities of a series of well-characterized nonheme oxoiron(IV) complexes and showed that the observed rates of oxidation depend on the nature of the supporting ligand and differ by over 6 orders of magnitude. The most reactive are represented by the S = 1 [Fe^{IV}(O)(Me$_3$NTB)] complex **11** (described by Nam),[63] the recently reported S = 2 [Fe^{IV}(O)(TQA)(NCMe)] complex **19**,[72] and the $Fe^{III,IV}_2$(TPA*) complexes **24** and **25** that have an S = 2 Fe^{IV}=O unit.[64,85,86] These observations emphasize that more remains to be learned about the factors that control the HAT reactivity, despite a consensus in the computational community that an S = 2 Fe^{IV}=O species is more reactive at HAT than its S = 1 counterpart.[49−55,78] In the second part, we report a further investigation of the HAT reactivity of **28**, the putative S = 2 Fe^{IV}=O oxidant generated from the reaction of **26a**/**26b** with dioxygen, and show that it is powerful enough to oxidize the strong C−H bonds of cyclohexane and even *n*-butane. The demonstration that **28** can hydroxylate *n*-butane represents the first example of a high-valent iron species derived from dioxygen that is capable of such a transformation. It not only provides a steppingstone toward our understanding of how metalloenzymes work but also highlights the potential such synthetic systems may hold.

EXPERIMENTAL SECTION

Materials and Methods. All reagents and solvents were purchased from commercial sources and used without further purification unless otherwise stated. The preparation and handling of air-sensitive materials were carried out under an inert atmosphere using a glovebox. The complexes [Fe(Tp^{Ph2})($O_2CC(O)Ph$)] (**26a**) and [Fe(Tp^{Ph2})($O_2CC(O)CH_3$)] (**26b**) were prepared as previously reported.[87]

Physical Methods. UV−vis spectra were recorded on a Agilent Cary 60 UV−vis spectrometer. Gas chromatography (GC) product analyses were performed on a PerkinElmer Autosystem XL gas chromatograph (AT-1701, 30 m; DB-1, 30 m) equipped with a flame ionization detector. GC−mass spectrometry (MS) analyses were performed on a Agilent 7890A gas chromatograph (HP-5MS, 30 m) equipped with an Agilent 5975C mass detector in electron impact mode. NMR analyses were recorded on a Bruker Avance 500 spectrometer.

Product Analysis. Organic products were analyzed after reaction with oxygen via GC: After the reaction, the mixture was passed through a short silica column and eluted with tetrahydrofuran. A known concentration of naphthalene was introduced into the reaction mixture as an internal standard. Yields of the oxidized products were determined by a comparison to authentic standards.

ASSOCIATED CONTENT

Supporting Information

Oxidation product ratios and yields and ^{1}H NMR spectra of butane-derived products. This material is available free of charge via the Internet at http://pubs.acs.org.

AUTHOR INFORMATION

Corresponding Author

*E-mail: larryque@umn.edu.

Notes

The authors declare no competing financial interest.

ACKNOWLEDGMENTS

This work was supported by National Science Foundation Grant CHE-1361773 to L.Q.

REFERENCES

(1) Crabtree, R. H. *Chem. Rev.* **2010**, *110*, 575−575.
(2) Vedernikov, A. N. *Acc. Chem. Res.* **2012**, *45*, 803−813.
(3) Que, L., Jr.; Tolman, W. B. *Nature* **2008**, *455*, 333−340.
(4) Sono, M.; Roach, M. P.; Coulter, E. D.; Dawson, J. H. *Chem. Rev.* **1996**, *96*, 2841−2887.
(5) Costas, M.; Mehn, M. P.; Jensen, M. P.; Que, L., Jr. *Chem. Rev.* **2004**, *104*, 939−986.

DOI: 10.1021/ic502786y
Inorg. Chem. 2015, 54, 5053−5064

(6) Conley, B.; Tenn, W., III; Young, K.; Ganesh, S.; Steve, M.; Oxgaard, J.; Gonzales, J.; Goddard, W., III; Periana, R. In *Activation of Small Molecules: Organometallic and Bioinorganic Perspectives*; Tolman, W., Ed.; Wiley-VCH: Weinheim, Germany, 2006; pp 235−285.
(7) Sheldon, R.; Arends, I.; Hanefeld, U. *Green Chemistry and Catalysis*; Wiley-VCH: Weinheim, Germany, 2007.
(8) Meunier, B. *Biomimetic Oxidations Catalyzed by Transition Metal Complexes*; Imperial College Press: London, 2000.
(9) Shaik, S.; Cohen, S.; Wang, Y.; Chen, H.; Kumar, D.; Thiel, W. *Chem. Rev.* **2010**, *110*, 949−1017.
(10) Dawson, J. H. *Science* **1988**, *240*, 433−439.
(11) Ortiz de Montellano, P. R. *Chem. Rev.* **2009**, *110*, 932−948.
(12) Denisov, I. G.; Makris, T. M.; Sligar, S. G.; Schlichting, I. *Chem. Rev.* **2005**, *105*, 2253−2277.
(13) Rittle, J.; Green, M. T. *Science* **2010**, *330*, 933−937.
(14) Wallar, B. J.; Lipscomb, J. D. *Chem. Rev.* **1996**, *96*, 2625−2657.
(15) Merkx, M.; Kopp, D. A.; Sazinsky, M. H.; Blazyk, J. L.; Muller, J.; Lippard, S. J. *Angew. Chem., Int. Ed.* **2001**, *40*, 2782−2807.
(16) Tinberg, C. E.; Lippard, S. J. *Acc. Chem. Res.* **2011**, *44*, 280−288.
(17) Beauvais, L. G.; Lippard, S. J. *J. Am. Chem. Soc.* **2005**, *127*, 7370−7378.
(18) Shu, L. J.; Nesheim, J. C.; Kauffmann, K.; Münck, E.; Lipscomb, J. D.; Que, L., Jr. *Science* **1997**, *275*, 515−518.
(19) Banerjee, R.; Proshlyakov, Y.; Lipscomb, J. D.; Proshlyakov, D. A. *Nature* **2015**, *518*, 431−434.
(20) Nesheim, J. C.; Lipscomb, J. D. *Biochemistry* **1996**, *35*, 10240−10247.
(21) Hausinger, R. P. *Crit. Rev. Biochem. Mol. Biol.* **2004**, *39*, 21−68.
(22) Koehntop, K. D.; Emerson, J. P.; Que, L., Jr. *J. Biol. Inorg. Chem.* **2005**, *10*, 87−93.
(23) Kappock, T. J.; Caradonna, J. P. *Chem. Rev.* **1996**, *96*, 2659−2756.
(24) Rocklin, A. M.; Tierney, D. L.; Kofman, V.; Brunhuber, N. M. W.; Hoffman, B. M.; Christoffersen, R. E.; Reich, N. O.; Lipscomb, J. D.; Que, L., Jr. *Proc. Natl. Acad. Sci. U.S.A.* **1999**, *96*, 7905−7909.
(25) Mirica, L. M.; Klinman, J. P. *Proc. Natl. Acad. Sci. U.S.A.* **2008**, *105*, 1814−1819.
(26) Baldwin, J. E.; Bradley, M. *Chem. Rev.* **1990**, *90*, 1079−1088.
(27) Roach, P. L.; Clifton, I. J.; Hensgens, C. M. H.; Shibata, N.; Schofield, C. J.; Hajdu, J.; Baldwin, J. E. *Nature* **1997**, *387*, 827−830.
(28) Schenk, W. A. *Angew. Chem., Int. Ed.* **2000**, *39*, 3409−3411.
(29) Krebs, C.; Fujimori, D. G.; Walsh, C. T.; Bollinger, J. M. *Acc. Chem. Res.* **2007**, *40*, 484−492.
(30) Riggs-Gelasco, P. J.; Price, J. C.; Guyer, R. B.; Brehm, J. H.; Barr, E. W.; Bollinger, J. M.; Krebs, C. *J. Am. Chem. Soc.* **2004**, *126*, 8108−8109.
(31) Price, J. C.; Barr, E. W.; Glass, T. E.; Krebs, C.; Bollinger, J. M. *J. Am. Chem. Soc.* **2003**, *125*, 13008−13009.
(32) Proshlyakov, D. A.; Henshaw, T. F.; Monterosso, G. R.; Ryle, M. J.; Hausinger, R. P. *J. Am. Chem. Soc.* **2004**, *126*, 1022−1023.
(33) Hoffart, L. M.; Barr, E. W.; Guyer, R. B.; Bollinger, J. M.; Krebs, C. *Proc. Natl. Acad. Sci. U.S.A.* **2006**, *103*, 14738−14743.
(34) Galonic, D. P.; Barr, E. W.; Walsh, C. T.; Bollinger, J. M.; Krebs, C. *Nat. Chem. Biol.* **2007**, *3*, 113−116.
(35) Fujimori, D. G.; Barr, E. W.; Matthews, M. L.; Koch, G. M.; Yonce, J. R.; Walsh, C. T.; Bollinger, J. M.; Krebs, C.; Riggs-Gelasco, P. J. *J. Am. Chem. Soc.* **2007**, *129*, 13408−13409.
(36) Matthews, M. L.; Krest, C. M.; Barr, E. W.; Vaillancourt, F. H.; Walsh, C. T.; Green, M. T.; Krebs, C.; Bollinger, J. M. *Biochemistry* **2009**, *48*, 4331−4343.
(37) Panay, A. J.; Lee, M.; Krebs, C.; Bollinger, J. M.; Fitzpatrick, P. F. *Biochemistry* **2011**, *50*, 1928−1933.
(38) Eser, B. E.; Barr, E. W.; Frantorn, P. A.; Saleh, L.; Bollinger, J. M.; Krebs, C.; Fitzpatrick, P. F. *J. Am. Chem. Soc.* **2007**, *129*, 11334−11335.
(39) Que, L., Jr. *Acc. Chem. Res.* **2007**, *40*, 493−500.
(40) McDonald, A. R.; Que, L., Jr. *Coord. Chem. Rev.* **2013**, *257*, 414−428.
(41) Ray, K.; Pfaff, F. F.; Wang, B.; Nam, W. *J. Am. Chem. Soc.* **2014**, *136*, 13942−13958.
(42) Nam, W.; Lee, Y.-M.; Fukuzumi, S. *Acc. Chem. Res.* **2014**, *47*, 1146−1154.
(43) Luo, Y.-R. *Comprehensive Handbook of Chemical Bond Energies*; CRC Press: Boca Raton, FL, 2007.
(44) Groves, J. T.; McClusky, G. A. *J. Am. Chem. Soc.* **1976**, *98*, 859−861.
(45) Shaik, S.; Kumar, D.; de Visser, S. P.; Altun, A.; Thiel, W. *Chem. Rev.* **2005**, *105*, 2279−2328.
(46) Kaizer, J.; Klinker, E. J.; Oh, N. Y.; Rohde, J.-U.; Song, W. J.; Stubna, A.; Kim, J.; Münck, E.; Nam, W.; Que, L., Jr. *J. Am. Chem. Soc.* **2003**, *126*, 472−473.
(47) Cho, K.-B.; Wu, X.; Lee, Y.-M.; Kwon, Y. H.; Shaik, S.; Nam, W. *J. Am. Chem. Soc.* **2012**, *134*, 20222−20225.
(48) Russell, G. *Reactivity, selectivity, and polar effects in hydrogen atom transfer reactions*; Wiley: New York, 1973.
(49) Finn, M.; Friedline, R.; Suleman, N. K.; Wohl, C. J.; Tanko, J. M. *J. Am. Chem. Soc.* **2004**, *126*, 7578−7584.
(50) Decker, A.; Rohde, J. U.; Klinker, E. J.; Wong, S. D.; Que, L., Jr.; Solomon, E. I. *J. Am. Chem. Soc.* **2007**, *129*, 15983−15996.
(51) Shaik, S.; Chen, H.; Janardanan, D. *Nat. Chem.* **2011**, *3*, 19−27.
(52) Wong, S. D.; Bell, C. B.; Liu, L. V.; Kwak, Y.; England, J.; Alp, E. E.; Zhao, J. Y.; Que, L., Jr.; Solomon, E. I. *Angew. Chem., Int. Ed.* **2011**, *50*, 3215−3218.
(53) Hirao, H.; Kumar, D.; Que, L., Jr.; Shaik, S. *J. Am. Chem. Soc.* **2006**, *128*, 8590−8606.
(54) Louwerse, M. J.; Baerends, E. J. *Phys. Chem. Chem. Phys.* **2007**, *9*, 156−166.
(55) Srnec, M.; Wong, S. D.; Solomon, E. I. *Dalton Trans.* **2014**, *43*, 17567−17577.
(56) Hirao, H.; Que, L., Jr.; Nam, W.; Shaik, S. *Chem.—Eur. J.* **2008**, *14*, 1740−1756.
(57) Mandal, D.; Ramanan, R.; Usharani, D.; Janardanan, D.; Wang, B.; Shaik, S. *J. Am. Chem. Soc.* **2015**, *137*, 722−733.
(58) Wilson, S. A.; Chen, J.; Hong, S.; Lee, Y. M.; Clémancey, M.; Garcia-Serres, R.; Nomura, T.; Ogura, T.; Latour, J. M.; Hedman, B.; Hodgson, K. O.; Nam, W.; Solomon, E. I. *J. Am. Chem. Soc.* **2012**, *134*, 11791−11806.
(59) Rohde, J. U.; In, J. H.; Lim, M. H.; Brennessel, W. W.; Bukowski, M. R.; Stubna, A.; Münck, E.; Nam, W.; Que, L. *Science* **2003**, *299*, 1037−1039.
(60) Sastri, C. V.; Lee, J.; Oh, K.; Lee, Y. J.; Jackson, T. A.; Ray, K.; Hirao, H.; Shin, W.; Halfen, J. A.; Kim, J.; Que, L., Jr.; Shaik, S.; Nam, W. *Proc. Natl. Acad. Sci. U.S.A.* **2007**, *104*, 19181−19186.
(61) Hong, S.; So, H.; Yoon, H.; Cho, K. B.; Lee, Y. M.; Fukuzumi, S.; Nam, W. *Dalton Trans.* **2013**, *42*, 7842−7845.
(62) Wang, D.; Ray, K.; Collins, M. J.; Farquhar, E. R.; Frisch, J. R.; Gómez, L.; Jackson, T. A.; Kerscher, M.; Waleska, A.; Comba, P.; Costas, M.; Que, L., Jr. *Chem. Sci.* **2013**, *4*, 282−291.
(63) Seo, M. S.; Kim, N. H.; Cho, K. B.; So, J. E.; Park, S. K.; Clémancey, M.; Garcia-Serres, R.; Latour, J. M.; Shaik, S.; Nam, W. *Chem. Sci.* **2011**, *2*, 1039−1045.
(64) Xue, G.; Pokutsa, A.; Que, L., Jr. *J. Am. Chem. Soc.* **2011**, *133*, 16657−16667.
(65) Lim, M. H.; Rohde, J. U.; Stubna, A.; Bukowski, M. R.; Costas, M.; Ho, R. Y. N.; Münck, E.; Nam, W.; Que, L. *Proc. Natl. Acad. Sci. U.S.A.* **2003**, *100*, 3665−3670.
(66) Company, A.; Prat, I.; Frisch, J. R.; Mas-Ballesté, R.; Güell, M.; Juhász, G.; Ribas, X.; Münck, E.; Luis, J. M.; Que, L., Jr.; Costas, M. *Chem.—Eur. J.* **2011**, *17*, 1622−1634.
(67) Planas, O.; Clémancey, M.; Latour, J.-M.; Company, A.; Costas, M. *Chem. Commun.* **2014**, *50*, 10887−10890.
(68) Hong, S.; Lee, Y. M.; Cho, K. B.; Sundaravel, K.; Cho, J.; Kirn, M. J.; Shin, W.; Nam, W. *J. Am. Chem. Soc.* **2011**, *133*, 11876−11879.
(69) Comba, P.; Wunderlich, S. *Chem.—Eur. J.* **2010**, *16*, 7293−7299.

DOI: 10.1021/ic502786y
Inorg. Chem. 2015, 54, 5053−5064

(70) England, J.; Martinho, M.; Farquhar, E. R.; Frisch, J. R.; Bominaar, E. L.; Münck, E.; Que, L., Jr. *Angew. Chem., Int. Ed.* **2009**, *48*, 3622−3626.
(71) England, J.; Guo, Y. S.; Van Heuvelen, K. M.; Cranswick, M. A.; Rohde, G. T.; Bominaar, E. L.; Münck, E.; Que, L., Jr. *J. Am. Chem. Soc.* **2011**, *133*, 11880−11883.
(72) Biswas, A. N.; Puri, M.; Meier, K. K.; Oloo, W. N.; Rohde, G. T.; Bominaar, E. L.; Münck, E.; Que, L., Jr. *J. Am. Chem. Soc.* **2015**, *137*, 2428−2431.
(73) England, J.; Bigelow, J. O.; Van Heuvelen, K. M.; Farquhar, E. R.; Martinho, M.; Meier, K. K.; Frisch, J. R.; Münck, E.; Que, L., Jr. *Chem. Sci.* **2014**, *5*, 1204−1215.
(74) Klinker, E. J.; Kaizer, J.; Brennessel, W. W.; Woodrum, N. L.; Cramer, C. J.; Que, L., Jr. *Angew. Chem., Int. Ed.* **2005**, *44*, 3690−3694.
(75) Klinker, E. J.; Shaik, S.; Hirao, H.; Que, L., Jr. *Angew. Chem., Int. Ed.* **2009**, *48*, 1291−1295.
(76) Zhou, Y. M.; Shan, X. P.; Mas-Ballesté, R.; Bukowski, M. R.; Stubna, A.; Chakrabarti, M.; Slominski, L.; Halfen, J. A.; Münck, E.; Que, L., Jr. *Angew. Chem., Int. Ed.* **2008**, *47*, 1896−1899.
(77) Ghosh, M.; Singh, K. K.; Panda, C.; Weitz, A.; Hendrich, M. P.; Collins, T. J.; Dhar, B. B.; Sen Gupta, S. *J. Am. Chem. Soc.* **2014**, *136*, 9524−9527.
(78) Kundu, S.; Thompson, J. V.; Shen, L. Q.; Mills, M. R.; Bominaar, E. L.; Ryabov, A. D.; Collins, T. J. *Chem.—Eur. J.* **2015**, *21*, 1803−1810.
(79) Janardanan, D.; Wang, Y.; Schyman, P.; Que, L., Jr.; Shaik, S. *Angew. Chem., Int. Ed.* **2010**, *49*, 3342−3345.
(80) Pestovsky, O.; Stoian, S.; Bominaar, E. L.; Shan, X. P.; Münck, E.; Que, L., Jr.; Bakac, A. *Angew. Chem., Int. Ed.* **2005**, *44*, 6871−6874.
(81) Pestovsky, O.; Bakac, A. *J. Am. Chem. Soc.* **2004**, *126*, 13757−13764.
(82) England, J.; Guo, Y. S.; Farquhar, E. R.; Young, V. G.; Münck, E.; Que, L., Jr. *J. Am. Chem. Soc.* **2010**, *132*, 8635−8644.
(83) Lacy, D. C.; Gupta, R.; Stone, K. L.; Greaves, J.; Ziller, J. W.; Hendrich, M. P.; Borovik, A. S. *J. Am. Chem. Soc.* **2010**, *132*, 12188−12190.
(84) Bigi, J. P.; Harman, W. H.; Lassalle-Kaiser, B.; Robles, D. M.; Stich, T. A.; Yano, J.; Britt, R. D.; Chang, C. J. *J. Am. Chem. Soc.* **2012**, *134*, 1536−1542.
(85) Xue, G.; De Hont, R.; Münck, E.; Que, L., Jr. *Nat. Chem.* **2010**, *2*, 400−405.
(86) Xue, G.; Geng, C.; Ye, S.; Fiedler, A. T.; Neese, F.; Que, L., Jr. *Inorg. Chem.* **2013**, *52*, 3976−3984.
(87) Mehn, M. P.; Fujisawa, K.; Hegg, E. L.; Que, L., Jr. *J. Am. Chem. Soc.* **2003**, *125*, 7828−7842.
(88) Mukherjee, A.; Martinho, M.; Bominaar, E. L.; Münck, E.; Que, L., Jr. *Angew. Chem., Int. Ed.* **2009**, *48*, 1780−1783.
(89) Tse, C. W.; Chow, T. W. S.; Guo, Z.; Lee, H. K.; Huang, J. S.; Che, C. M. *Angew. Chem., Int. Ed.* **2014**, *53*, 798−803.
(90) Vincent, J. B.; Huffman, J. C.; Christou, G.; Li, Q.; Nanny, M. A.; Hendrickson, D. N.; Fong, R. H.; Fish, R. H. *J. Am. Chem. Soc.* **1988**, *110*, 6898−6900.

DOI: 10.1021/ic502786y
Inorg. Chem. 2015, 54, 5053−5064